

Article

# Neutron Activation Analysis for Geochemical Characterization of Rocks from Gold Mines in Egypt

Wael M. Badawy <sup>1,2,\*</sup>, Mohamed Mitwalli <sup>3</sup>, Andrey Yu. Dmitriev <sup>2</sup>, Olesia Chepurchenko <sup>2</sup>, Gehad Saleh <sup>4</sup>, Ali El-Farrash <sup>3</sup>, Maksim Bulavin <sup>2</sup>, Tarek Morsi <sup>1</sup> and Mohammed Sallah <sup>3,5,\*</sup>

<sup>1</sup> Radiation Protection and Civil Defense Department, Nuclear Research Centre, Egyptian Atomic Energy Authority, Cairo 13759, Egypt

<sup>2</sup> Frank Laboratory of Neutron Physics, Joint Institute for Nuclear Research, Dubna 141980, Russia

<sup>3</sup> Physics Department, Faculty of Science, Mansoura University, Mansoura 35516, Egypt

<sup>4</sup> Nuclear Materials Authority, El-Maadi, P.O. Box 530, Cairo 11381, Egypt

<sup>5</sup> Higher Institute of Engineering and Technology, New Damietta 34517, Egypt

\* Correspondence: wael@jinr.ru (W.M.B.); msallahd@mans.edu.eg (M.S.)

**Abstract:** The present work was carried out to determine the elemental composition of granitoid rock samples from three gold mines (Sukari, Hamash, and Um Hagalig) in the South-eastern part of Egypt and quantification of the extent of the elemental enrichment. A total of 37 samples from the mines were subjected to neutron activation analysis, and the mass fractions of the elements were measured in mg/kg. The results show a dominance of K (76.9%), Fe (11.0%), Ca (8.7%), and Na (3.1%) for Sukari mine; Na (31.2%), Ca (28.5%), K (23.1%), and Fe (9.9%) for the Hamash mine; and for the Um Hagalig mine Na (31.1%), K (22%), Ca (21.7%), and Fe (20.8%). In addition, significant mass fractions of uranium, thorium and rare earth elements were found in Hamash and Um Hagalig. The average mass fractions of U in the investigated areas are measured to be 59.7, 48.2, and 30.8 mg/kg for Hamash, Sukary, and Um Hagalig, respectively. Furthermore, the average mass fractions of Th were significant and measured to be 3905, 1673, and 7 mg/kg for Hamash, Um Hagalig, and Sukary, respectively. Multiple ratio indicators and discrimination diagrams were used to better understand the origin of the elements in the samples studied. The indicators suggest that the provenance of the elements is mainly from metavolcanic and volcanic rocks. The findings should make an important contribution to the study of ores and minerals and thus represent an important area for environmental studies.

**Keywords:** elemental composition; gold mines; neutron activation analysis; ratio indicators; metavolcanics and younger granite



**Citation:** Badawy, W.M.; Mitwalli, M.; Dmitriev, A.Y.; Chepurchenko, O.; Saleh, G.; El-Farrash, A.; Bulavin, M.; Morsi, T.; Sallah, M. Neutron Activation Analysis for Geochemical Characterization of Rocks from Gold Mines in Egypt. *Appl. Sci.* **2023**, *13*, 4564. <https://doi.org/10.3390/app13074564>

Academic Editor: Jianbo Gao

Received: 11 March 2023

Revised: 1 April 2023

Accepted: 1 April 2023

Published: 4 April 2023



**Copyright:** © 2023 by the authors. Licensee MDPI, Basel, Switzerland. This article is an open access article distributed under the terms and conditions of the Creative Commons Attribution (CC BY) license (<https://creativecommons.org/licenses/by/4.0/>).

## 1. Introduction

Numerous gold-bearing quartz veins formed as a result of tensional or transgressional shearing, when the encircling neighborhood rocks were crumpled and/or reverse-disparaged [1,2]. The geometry and kinematics of gold-bearing quartz veins in Egypt's Central Eastern Desert (CED) have been explained using transgression involving oblique convergence [3,4]. Technologically advanced gold mining in Egypt was launched in 2009, particularly in the Sukari gold mine, which is located about 25 km from the Red Sea. The strategic credit of Sukari has 13.7 million ounces (388,395 kg) of evaluated and demonstrated resources and 2.3 million ounces (65,205 kg) of inferred resources, according to Mineral Resource and Mineral Reserve Estimate for the Sukari Gold Project, Centamin Company, an Australian mining operator [5–7]. A detailed description of the structural setting of the mines and the geological processes that led to the formation of Au-bearing ores is published elsewhere by Helmy et al. [8].

Furthermore, the medium-scale production from the Hamash mine was noticed, which came on stream in 2010 through the joint national Hamash Egypt for Gold Mines project. Several exploration and diamond drilling projects are also under construction in

other investigation locations of the CED. The Hamash gold mine area (HGMA) is located 100 km west of Marsa Alam on the Red Sea coast and 40 km south of the line linking Marsa Alam and Edfu cities. The previous integrated work of Sukari Gold Mine (SGM) focused on remote sensing data along with geochemical and isotopic analyses to assess the environmental impacts of (the SGM) observations mining process [9].

Since ancient times, the Egyptian Eastern Desert has been renowned as a gold mining location. More than 90 old gold mines are distributed across the region, with the largest in its central and southern areas [4,10–16]. Few studies have been conducted to extract information on the genesis and sort of gold mineralization and geochemical characterization, as reported by El-Desoky, Shahin, and Amer [10]. The authors determined the mass fractions of thirty-four elements, and the average value of gold was determined to be 0.74 ppm. Furthermore, the researchers found that the presence of granites and quartz veins at the Hamash mine, which is N.W. and N.S. host trending, is related to the presence of gold.

The samples from the investigated areas (Sukari, Hamash, and Um Hagalig) were examined in terms of their geochemistry using neutron activation analysis. Neutron activation analysis (NAA) differs from other analytical methods in its precision, accuracy, sensitivity, and nondestructive analysis technique. More details about NAA were published elsewhere [17–23].

The main objectives of the present work can be summarized as; (i) determining the elemental composition of the studied granitoid rock samples (abundances and correlation), (ii) studying the provenance of the granitoid rocks based on the obtained geochemical data using ratio indicators, and discrimination diagrams and (iii) calculating the enrichment factors as integrative factors highlighting the significant elements' enrichment and the geo-accumulation index as well.

## 2. Materials and Methods

### 2.1. Sampling Strategy

The investigated granitoid rock samples of 200 g from each location were collected from the vicinity of the Sukari, Hamash, and Um Hagalig gold mines areas, as shown in Figure 1. A total of 37 samples were collected from the three mines (#17 from Sukari, #11 from Hamash, and #9 from Um Hagalig). A detailed description of the locations, the corresponding coordinates, and the features are provided in Table S1 Supplementary Materials. The sampling procedures followed the recommended protocol from the Geological Survey and Mining Authority of Egypt, and the guidelines in TECDOC-1415 for the sampling of environmental contaminants [24].

### 2.2. Geological Features

The Sukari gold mine is located about 15 km southwest of Marsa Alam, between the Red Sea coast and the Hafafit gneiss-dome, as shown in Figure 2. The mine occurs within a Late Neoproterozoic granitoid that intruded volcanic-sedimentary sequences and an ophiolitic mass known as Wadi Ghadir Melange. The volcanic-sedimentary succession consists of andesites, dacites, rhyodacite, and pyroclastic. The volcanic rocks are calcareous and were formed in an island-arc environment. The ophiolitic sequence is represented by a serpentinite at the base, followed by a metagabbro–diorite complex and layered veins. Metagabbro–diorite rocks and serpentinites form lenticular bodies (13 km<sup>2</sup>), as well as small bodies conformably scattered throughout the volcanic-sedimentary sequence. All rocks are weakly metamorphosed (lower greenschist metamorphic facies), strongly sheared, and altered into various schists along shear zones. Mineralized quartz veins and talc–carbonate veins are common [8,25].

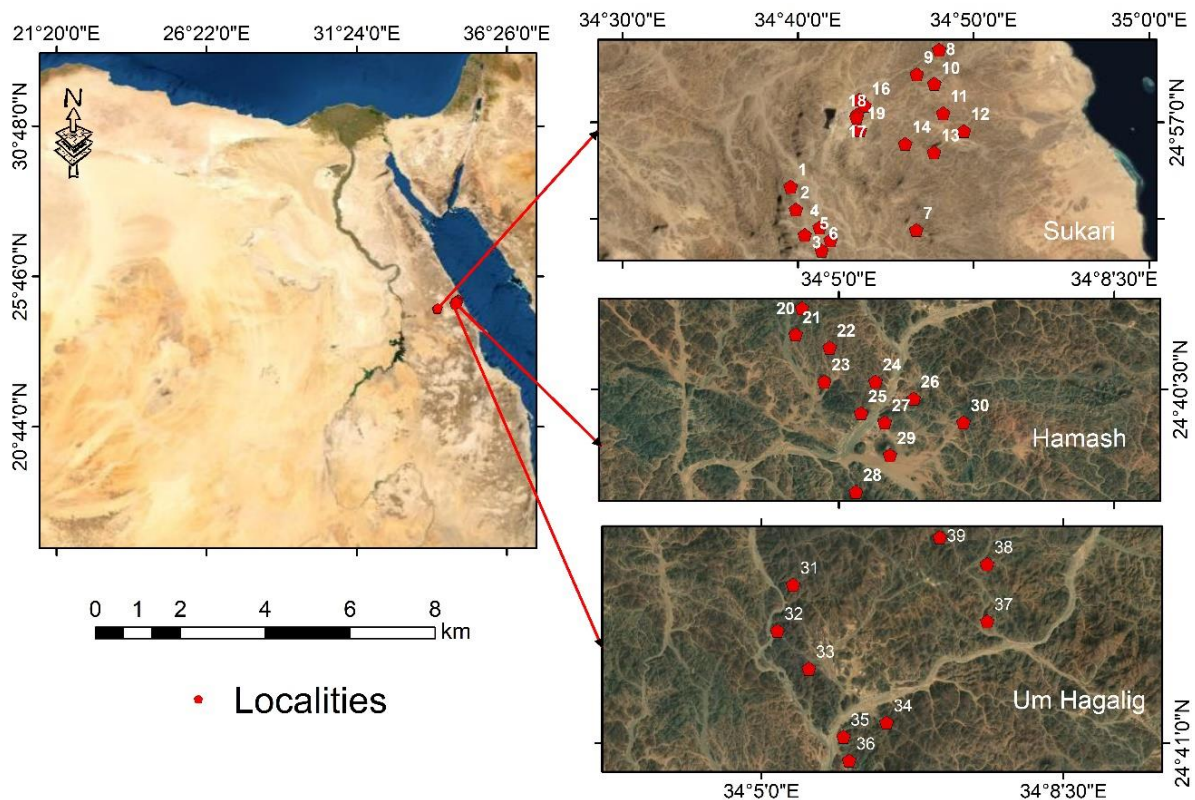


**Figure 1.** The map of localities of the studied areas.



**Figure 2.** Field pictures from the Sukari gold mine and signed arrows show the location of some collected samples (younger granite).

Sukari granitoid, as in Figure 2, is elongated in the NNE-SSW orientation and is limited to the west and east by two severe shear zones, totaling about 10 km<sup>2</sup>. The younger rock is leucocratic, coarse-grained, and pink in color. Its mineralogical composition is varied, ranging from granodiorite to monzogranite, with quartz, plagioclase, feldspar, and biotite [8].

Likewise, the geological features of the Hamash mine are given in Figure 3, which is divided into two zones: the mine itself and Um Hagalig. The HGM region has low and medium relief terrain. Multiple wadis pierce it to the northwest NW-SE of the Hafafit gneiss-dome and the south of the Baramiya ophiolite belt. According to fieldwork, the study area is primarily made up of Neoproterozoic rocks such as island-arc related metavolcanic

and meta-volcanoclastic rocks, syn- to late-orogenic granites (granodiorites and alkali feldspar granites), and trachyte rocks intruded by a group of drifts and quartz veins [10].



**Figure 3.** Field pictures from the Hamash gold mine and signed arrows show the location of collected samples (metavolcanic rocks on the left and younger granite on the right).

At about 780–750 Ma, the metavolcanic rocks are the oldest and consist mostly of basalt and andesite coupled with Meta volcanoclastic rocks of low-grade schists, mudstones, and amphibolite rocks. Metavolcanic rocks are fine-grained, greyish-green in appearance, and feature porphyritic textures at times. The rocks are foliated, folded, and fractured, and they trend NNW-SSE. The meta-andesite is composed of plagioclase and hornblende as massive phenocrysts with little pyroxene buried in a fine-grained groundmass comprising plagioclase laths, amphiboles, and opaque minerals. Plagioclase, pyroxene, amphibole, and olivine relicts dominate the metabasaltic. Secondary minerals include sericite, chlorite, epidote, and carbonate minerals.

### 2.3. Sample Preparation and Analysis Using (NAA)

Samples were taken to the laboratory for processing. They were ground with an agate mortar and passed through a 100  $\mu\text{m}$  sieve. The resulting cleaned and pulverized samples were dried at 104  $^{\circ}\text{C}$  for 24 h until they reached a constant weight. Aliquots of approximately 0.1 g were used for both powdered samples and certified reference materials. After weighing, each sample was packed into aluminum cups, labeled, and wrapped with aluminum foil. They were then stored in a desiccator with other prepared samples. Close-up images of fragments from the studied mines are shown in Figure 4.

The prepared samples were subjected to NAA at the IBR-2 reactor FLNP, JINR. An average power of 1.6 MW was used to irradiate the samples through the 3rd channel of the pulsed nuclear reactor of FLNP. Detailed features of the channel were published elsewhere [26–29]. Fluxes of thermal and resonance neutrons  $\Phi_{\text{th}} = 7.88 \times 10^{11} \text{ n/cm}^2 \text{ s}$  and  $\Phi_{\text{res}} = 2.43 \times 10^{11} \text{ n/cm}^2 \text{ s}$ , respectively, were utilized to irradiate the samples. Afterward, the samples were kept for a period of 3–5 days until the induced radioactivity had decayed, making them safe to handle. Upon repackaging the samples, a gamma-ray spectrometer was used to evaluate the induced radioactivity of the long-lived isotopes for a duration of 30 and 90 min for the 1st and the 2nd long-lived isotopes, respectively.

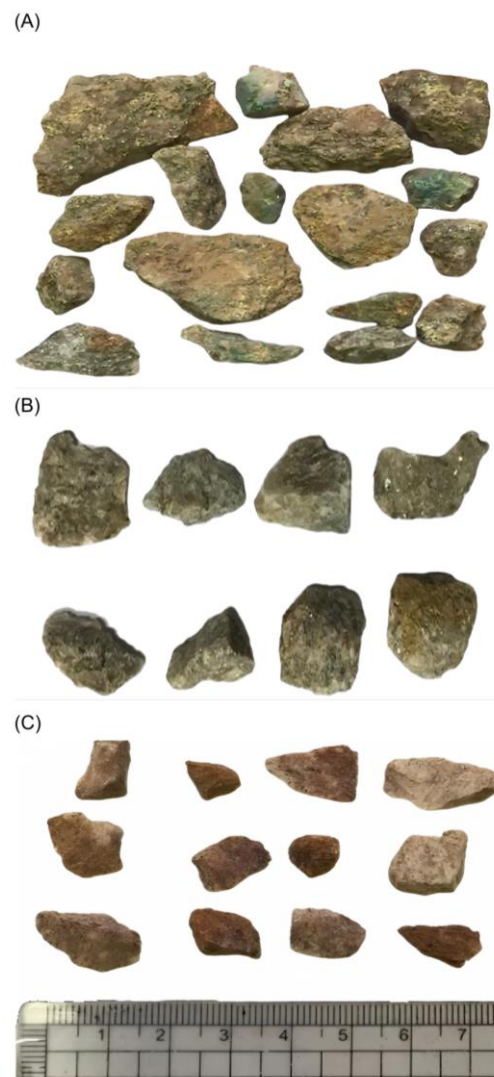


**Figure 4.** Fragment rocks from the investigated gold mines; Sukari (A), younger granite, Hamash (B), metavolcanic rocks, and Um Hagalig (C), younger granite.

For measuring the induced radioactivity, a high-purity germanium (HPGe) detector was employed, which has a resolution of 2.1 keV for the 1332 keV line of the  $^{60}\text{Co}$ . CANBERRA Genie 2000 software v 3.4 was used to accumulate and analyze the obtained spectra. The mass fractions of elemental content in mg/kg of the rock samples was calculated using a software developed by Dmitriev and Pavlov [30].

### 3. Quality Control

Certified reference materials were used to conduct quality control on the samples, which included NIST SRM 1633c—Coal Fly Ash, NIST SRM 2706—Trace Elements in Soil, NIST SRM 1835—Trace Elements in borate ore, NIST SRM 1632E—Trace Elements in Coal, NIST SRM 2709A—baseline Trace Element concentrations in San Joaquin Soil, and NIST SRM 2710A—Montana I Soil. The relative standard error was determined to be between 1–20% for most of the materials, except for Yb, Hf, and Zr, which exhibited higher levels exceeding 20%.

### 4. Statistical Data Analysis

The R statistical software package (R 4.2.2) was used for all statistical analyses of chemical data, including infographics [31]. The data were handled in an M.S. Excel sheet, and the normal distribution of the data was tested using the Shapiro-Wilk test [32]. The

complete set of elements was investigated with a probability of 95% and ( $p \leq 0.05$ ). Furthermore, the analysis of variance (ANOVA) was carried out, and the most common Tukey's Honestly Significant Difference (Tukey's HSD) post-hoc test [33,34] was used to specifically differentiate the mean differences between the three studied mines. The locations of the analysed samples were mapped using GIS technology. The descriptive statistics for each sector were calculated. The inter-correlation coefficients were extracted and plotted. The ratio indicators were computed to extract more information about the rock samples' origin.

## 5. Results and Discussion

### 5.1. Elemental Composition and Inter-Correlation

The descriptive statistics of the mass fractions of the determined elements are given in detail in Table 1. A total of 34, 26, and 33 elements were determined for Sukari, Hamash, and Um Hagalig, respectively. For the Sukari mine, the maximum mass fraction was measured for K with a mean value of 213,376 mg/kg, whereas the minimum value was noticed for Au with a mean value of 0.0026 mg/kg.

Similarly, the maximum value was computed for Na in Hamash with an average value of 41,581 mg/kg. In comparison, the minimum value was calculated for Au with a mean value of 0.0081 mg/kg. Finally, the maximum value for Um Hagalig was found for Na, with a mean value of 35,644 mg/kg, and the minimum value of 0.0046 mg/kg was noticed for Au.

All the obtained mass fractions in mg/kg of the common elements in the three studied mines are plotted in Figure 5. At first glance, the figure depicts that the mass fractions of Hamash are higher than those of others in the case of rare earth elements.

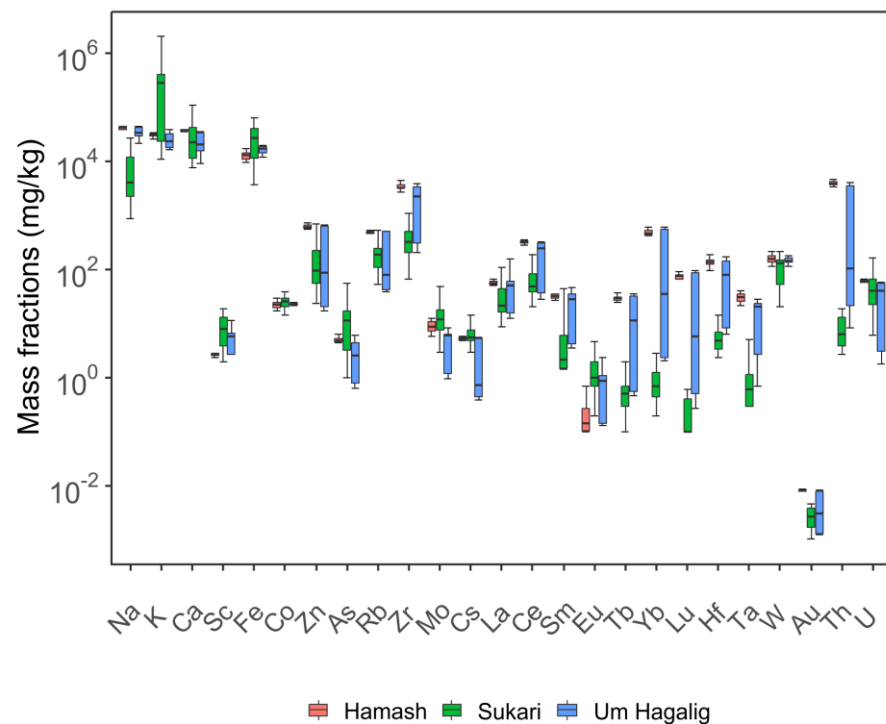


**Figure 5.** Mass fractions of the determined elements in the investigated mines.

**Table 1.** Mean, median, and median absolute deviation of the elemental composition of the studied areas. All the mass fractions are expressed in mg/kg (*n* = 37).

Element	Sukari			Hamash			Um_Hagalig			[10]
	Mean ± SE	Median ± MAD	Min-Max	Mean ± SE	Median ± MAD	Min-Max	Mean ± SE	Median ± MAD	Min-Max	
Na	8493 ± 2349	2970 ± 3106	868–27,600	41582 ± 1157	42,600 ± 3558	32,400–45,700	35,644 ± 2676	34,500 ± 10,526	21,600–44,500	2670
K	213,376 ± 50,562	204,000 ± 270,575	10,800–683,000	30836 ± 694	30,900 ± 2520	25,900–34,200	25,222 ± 2765	23,400 ± 9637	16,300–38,300	19,093
Ca	24,091 ± 3535	22,300 ± 16,902	7620–49,400	37918 ± 537	38,200 ± 1334	33,600–39,900	24879 ± 3576	20700 ± 17035	9210–36,600	26,872
Sc	10.0 ± 1.3	9 ± 7	2.0–19.2	2.8.0 ± 0.1	0.4 ± 15.9	2.7 ± 0.7	5.3 ± 1	5.7 ± 4.3	2.7–11.5	13
Cr	85.0 ± 15.1	105 ± 59	5.6–178.0	ND	ND	ND	33 ± 14	20 ± 5	15–141	17.5
Fe	30,459 ± 5101	27,500 ± 29,830	3660–64,500	13135 ± 708	13,300 ± 2965	9790–17,600	23,767 ± 7606	17600 ± 4596	12,000–84,200	34,977
Ni	30.0 ± 6.5	27 ± 17	1.5–99.1	ND	ND	ND	20 ± 1	20 ± 6	14–25	16
Co	29.0 ± 2.7	27 ± 9	17.6–64.8	23 ± 1	22 ± 4	17–29	24 ± 1	24 ± 1	21–28	ND
Zn	114 ± 23	78 ± 44	23.5–352.0	610 ± 27	609 ± 62	390–724	303 ± 106	88 ± 105	17–672	41.9
Se	0 ± 0	0 ± 0	0.0–0.5	ND	ND	ND	ND	ND	ND	ND
As	13.0 ± 3.4	11 ± 11	1.0–56.5	4.9 ± 0.2	4.9 ± 0.5	3.4–6.3	3 ± 0.8	2.6 ± 2.8	0.7–6.1	14.9
Br	1.0 ± 0.2	1 ± 1	0.3–2.2	ND	ND	ND	ND	ND	ND	ND
Rb	168 ± 19	147 ± 86	53.7–307.0	484 ± 11	491 ± 22	390–531	294 ± 41	359 ± 96	107–424	96.2
Sr	167 ± 22	167 ± 87	19.6–329.0	ND	ND	ND	1918 ± 539	2320 ± 2372	208–3920	52.9
Zr	366.0 ± 66.5	324 ± 236	68–1110	3365 ± 162	3260 ± 460	2430–4410	4.4 ± 1.0	6.1 ± 3.4	1–8.4	186.7
Mo	12.0 ± 1.8	10 ± 4	2.1–31.6	9.0 ± 0.7	8.6 ± 2	5.9–12.4	0.8 ± 0.3	0.3 ± 0.3	0.1–2.6	1.57
Sn	24.0 ± 4.7	20 ± 24	1.5–57.9	ND	ND	ND	38 ± 12	26 ± 13	17–131	ND
Sb	1.0 ± 0.2	1 ± 1	0.1–2.2	ND	ND	ND	0.3 ± 0.0	0.4 ± 0.1	0.1–0.4	0.37
Ba	239 ± 32	220 ± 133	48.4–502.0	ND	ND	ND	322 ± 84	265 ± 283	74–591	151.5
Cs	7.0 ± 0.9	7 ± 3	3.0–17.6	5.3 ± 0.1	5.4 ± 0.3	4.5–5.9	2.7 ± 0.9	0.7 ± 0.5	0.4–5.6	ND
La	30.0 ± 6.1	21 ± 7	8.6–111.0	56 ± 2	57 ± 8	41–66	50 ± 15	52 ± 52	13–156	5.7
Ce	61.0 ± 10.9	42 ± 19	20.7–186	325 ± 15	323 ± 33	218–428	184 ± 48	253 ± 113	28–329	14.7
Nd	26.0 ± 4.7	21 ± 15	6.6–81.0	ND	ND	ND	52 ± 19	52 ± 39	4–196	10.6
Sm	3.0 ± 0.7	2 ± 2	0.0–10.5	31 ± 2	32 ± 4	17–36	22 ± 6	29 ± 27	3–47	3
Eu	1.0 ± 0.3	1 ± 0	0.2–4.7	0.3 ± 0.1	0.1 ± 0.1	0.1–0.7	0.8 ± 0.3	0.9 ± 1.1	0.1–2.3	0.56
Tb	1.0 ± 0.1	0 ± 0	0.1–2.0	28 ± 2	29 ± 4	12–36	16 ± 5	12 ± 17	0–35	ND
Yb	1.0 ± 0.2	1 ± 0	0.2–2.8	471 ± 32	465 ± 68	200–609	253 ± 97	35 ± 49	2–605	3.55
Lu	0 ± 0	0 ± 0	0.0–0.6	72 ± 5	75 ± 10	30–92	39 ± 15	6 ± 8	0–94	ND
Hf	5.0 ± 0.9	5 ± 2	0.6–14.1	139 ± 8	139 ± 22	94–190	79 ± 23	82 ± 100	6–169	ND
Ta	1.0 ± 0.3	0 ± 0	0.3–5.0	30 ± 2	31 ± 8	16–41	14 ± 4	20 ± 11	1–28	ND
W	115.0 ± 15.2	125 ± 90	20.5–214.0	160 ± 9	155 ± 27	116–212	141 ± 11	144 ± 36	67–178	ND
Au	$2.6 \times 10^{-3} \pm 2.7 \times 10^{-4}$	$2.7 \times 10^{-3} \pm 1.5 \times 10^{-3}$	$1.0 \times 10^{-3} \pm 4.6 \times 10^{-3}$	$8.1 \times 10^{-3} \pm 1.9 \times 10^{-4}$	$8.1 \times 10^{-3} \pm 3.4 \times 10^{-4}$	$6.4 \times 10^{-3} \pm 8.7 \times 10^{-3}$	$4.6 \times 10^{-3} \pm 1.1 \times 10^{-3}$	$3.0 \times 10^{-3} \pm 2.7 \times 10^{-3}$	$1.2 \times 10^{-3} \pm 8.4 \times 10^{-3}$	0.74
Th	7.0 ± 1.3	5 ± 3	2.7–19.1	3905 ± 169	3990 ± 519	2750–4740	1673 ± 649	105 ± 143	8–4020	0.8
U	48.0 ± 10.2	39 ± 42	3.5–168.0	60 ± 2	61 ± 3	42–68	31 ± 9	40 ± 28	2–59	0.5

ND = not detected, MAD = Median absolute deviation.

In addition, the elements with the highest mass fractions (K, Ca, Fe, and Na); (Na, Ca, K, Fe, Th, and Zr); (Na, K, Ca, Fe, and Th) were determined for Sukari, Hamash, and Um Hagalig, respectively. The Shapiro–Wilk test of normality was performed. Most of the obtained mass fractions of the elements are not normally distributed. For instance, for the Sukari mine, all the elements are not normally distributed except Ba, Sr, Rb, Sc, Au, Se, Br, W, Sb, and Mo. Contrariwise, for the Hamash mine, all the elements are normally distributed except Sc, Rb, Ag, Sm, Eu, Tb, Yb, Lu, Au, and U. The obtained results of the normality test suggest a further statistical treatment of the data before shaping any hypothesis or interpretation [35]. The analysis of variance (ANOVA) was calculated, and the most common Tukey’s Honestly Significant Difference (Tukey’s HSD) post-hoc test was used to differentiate the mean differences between the investigated mines. In the present work, three models, namely one-way ANOVA, two-way ANOVA, and interaction of analysis of variance, were computed and tested for the best model. Akaike’s Information Criterion (AIC) was used to select the best model [36]. The model with the lowest AIC value is considered the best, and in the present work, the best model was the interaction one. Accordingly, ANOVA results show that there is little statistically significant difference concerning the investigated mines ( $p$ -value = 0.006  $\leq$  0.05). Contrariwise, the results show that there is a statistically significant difference and failure to reject the null hypothesis concerning the determined elements ( $p$ -value  $\leq$  0.001) and the interaction element and mines ( $p$ -value  $\leq$  0.001). Specifically, Tukey’s test shows that there are no statistically significant differences in the mean values of the elemental composition of the studied mines as the probabilities were calculated to be 0.028, 0.96, and 0.018 for Sukari–Hamash, Um Hagalig–Hamash, and Um Hagalig–Sukari, respectively. These findings prove the fact of the similarity of granitic rock samples collected from Hamash and Um Hagalig in terms of the geochemical features.

The correlation coefficients were extracted based on the Pearson method. The highest correlation coefficients were noticed for some pairs, specifically, Yb:Lu, Au:Th, and Tb:Yb ( $r > 0.99$ ) for the Sukari mine, whereas for the Hamash mine, the highest correlated pairs were noticed for Co:W, Yb:Lu, Au:U, Au:Sm, and Zn:Rb ( $r > 0.90$ ). Finally, for Um Hagalig, the most linked pairs are calculated to be Yb:Lu, Sc:Eu, Rb:Cs, and Zn:Th ( $r > 0.99$ ). It seems that the highest correlation coefficients were calculated between the rare earth elements (REE). The results obtained from REE are largely consistent with the corresponding values obtained from Roshdy et al. [37] from Phosphate mines. In addition, there is a good correlation between Au and U at the Hamash mine. This finding proves a significant association between the two elements in the mine and again suggests that attention should be paid to this feature.

## 5.2. Trace Element Geochemistry

For a better understanding of the provenance of the trace elements, informative ratio indicators were implemented to extract information about their origin. To check the degree of metavolcanics and younger granite recycling, the ratio of Zr/Sc versus Th/Sc was used. The ratio indicator is plotted in Figure 6. It is apparent from the figure that there is a considerable degree of Zr enrichment for Hamash, where the results of the ratio indicator were calculated to be (1241 versus 1452). In addition, it was calculated for Um Hagalig to be (601 versus 606). Finally, the lowest ratio was calculated for the Sukari mine to be (184 versus 170). For comparison purposes, the same ratio indicator was calculated from the literature to be (6.6 versus 0.41) for North American shale composite NASC as it was reported by Gromet et al. [38], (22.8 versus 0.8) for world soil average WSA by Kabata-Pendias [39], (13 versus 0.9) for Post Archean Australia Shale PAAS by Taylor and McLennan [40], and (13.8 versus 0.75) for upper continental crust UCC by Rudnick and Gao [41], respectively. The obtained results of Hamash and Um Hagalig show that there are significant metavolcanics and younger granite recycling, whereas the results of the Sukari mine are close to the corresponding values of UCC, NASC, and WSA. These findings show that there is noticeable metavolcanics and younger granite recycling.

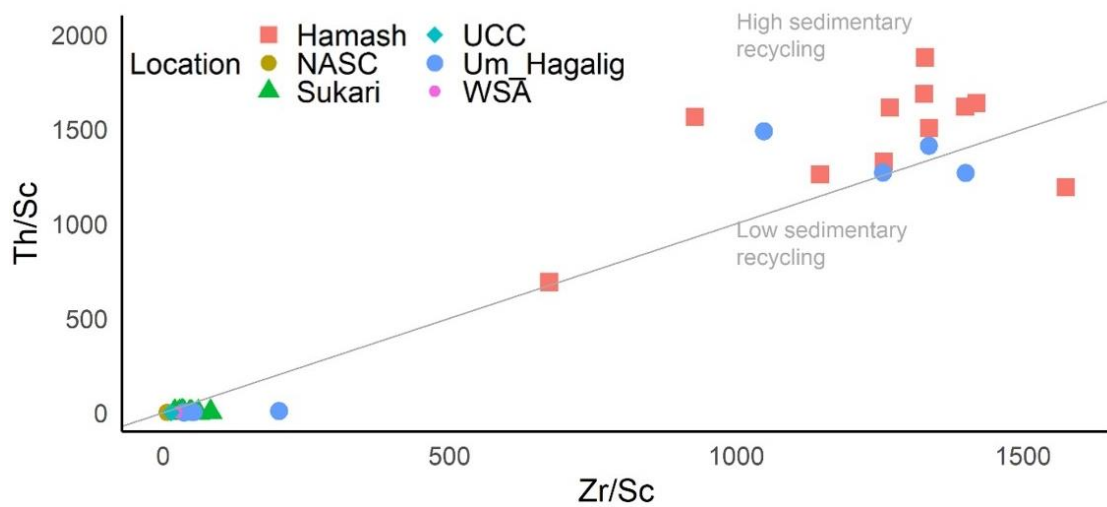


**Figure 6.** Th/Sc vs. Zr/Sc relationship showing Zr enrichment and proving high sediment recycling in Hamash. The corresponding values from the literature were provided. The values were reported by Rudnick and Gao [41] for upper continental crust UCC, Gromet, Haskin, Korotev, and Dymek [38] for North American shale composite NASC, Taylor, and McLennan [40] for Post Archean Australia Shale PAAS, and Kabata-Pendias [39] for world soil average WSA. Background after Bhatia and Crook [42].

Another informative ratio indicator is the relationship between Th and U, and this is clearly plotted and illustrated in Figure 7. This ratio was chosen as an indicator of the enrichment or depletion of Th and U. The ratio indicator proves the obtained findings as the previous one and shows that significant amounts of Th and U are noticed in the studied samples collected from the Hamash mine (Th/U = 65.5). A considerable amount of Th and U was noticed for Um Hagalig (Th/U = 32.5) as well. Unlike the Hamash and Um Hagalig mines, the Sukari mine has a relatively less amount (Th/U = 8.0) compared with the corresponding values in UCC (Th/U = 3.9), NASC (Th/U = 4.6), PAAS (Th/U = 4.7), and WSA (Th/U = 3.1).

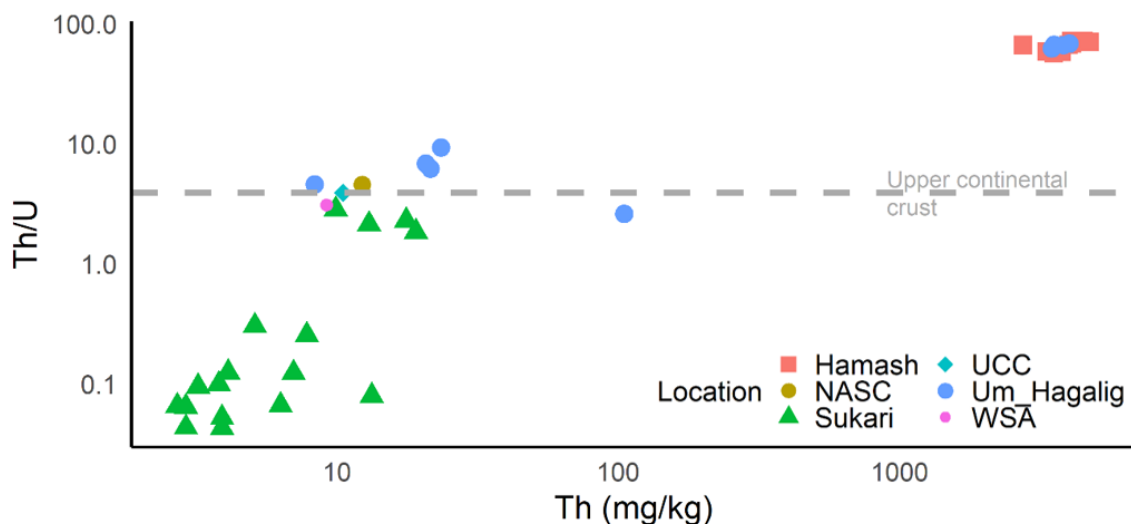


**Figure 7.** The biplot illustrating the relationship between Th/U vs. Th. For comparison purposes, the corresponding values reported by Rudnick and Gao [41] for upper continental crust UCC, Gromet, Haskin, Korotev, and Dymek [38] for North American shale composite NASC, Taylor and McLennan [40] for Post Archean Australia Shale PAAS, and Kabata-Pendias [39] for world soil average WSA.

Based on the obtained results, the Hamash mine has a considerable amount of uranium and thorium ores that could be of great fortune for the country, and attention should be paid to that mine for not only gold mining but as uranium and thorium sources as well [16]. These peculiarities most likely prove that both U and Au have an origin in magmas as U is leached out of granite by fluids and precipitates when the fluids encounter carbon, e.g., in graphite. When magmas intrude/extrude into an area of mafic volcanic rocks, their Au-bearing fluids can leach further gold from the (mafic) volcanic rocks and precipitate in native form or pyrite [10,43,44].

In the case of metavolcanics and younger granite rocks, researchers have recommended other discrimination diagrams based on Si that could serve as a better tool to clarify and distinguish between different rocks [45,46]. In the present work, however, the discrimination diagram proposed by Pearce, Harris, and Tindle [47] was obviously the proper one to distinguish the granitic rocks. Therefore, one more helpful ratio that is widely used to differentiate the origin of granitic rocks is the relationship between Th/Ta versus Yb (mg/kg) [47,48].

It is clear from Figure 8 that there are significant mass fractions of Th in the Hamash mine over the Sukari and Um Hagalig ones. The later mines also have considerable amounts of Th but less than the Hamash one. The ratio of Th/Ta is calculated to be 137.3, 29.8, and 73.4 for the Hamash, Sukari, and Um Hagalig mines, respectively. The obtained results are much lower than those reported for NASC (10.98) by Gromet, Haskin, Korotev, and Dymek [38], WSA (6.62) by Kabata-Pendias [39], and UCC (11.66) by Rudnick and Gao [41]. The figure depicts that most of the Hamash rocks are located near oceanic arcs, whereas Sukari and Um Hagalig are located on the active continental margin. Therefore, the results obtained are comparable to the geochemistry of arc-related felsic volcanic rocks for Hamash and active continental margin for Sukari and partially for Um Hagalig. There is good agreement between the ratio indicators.

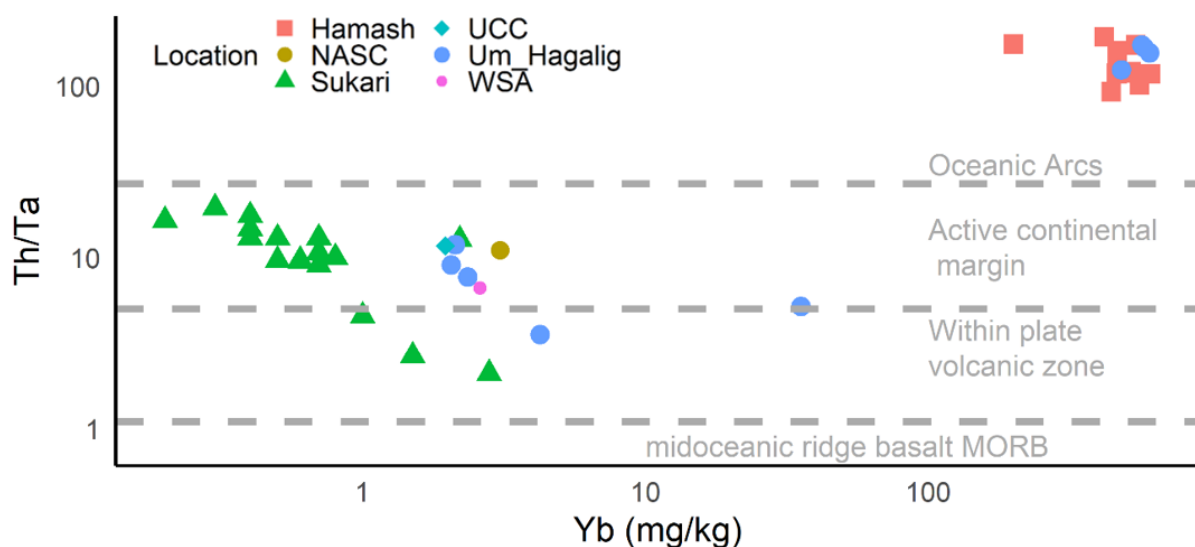


**Figure 8.** Th/Ta versus Yb relationship in which felsic volcanic rocks of mines are close to the fields of oceanic arc and active continental margin [47]. After Pearce, Harris, and Tindle [47].

These peculiarities confirm that these discrimination diagrams are helpful and informative to sort and classify the analyzed samples based on the geochemical data [48]. The discrimination diagrams show their efficiency and suitability in classification and distinguishing the obtained elements based on the geochemical data. In addition to that, an effective discriminatory diagram was used to extract information about the provenance by using ternary diagrams of La-Th-Sc and Th-Zr/10-Sc.

The ternary diagrams of the ratios were plotted as clearly illustrated in Figure 9A,B. From Figure 9A, the collected samples from Sukari and Um Hagalig are scattered relative

to UCC, NASC, PAAS, and WSA, whereas Hamash is located far from the other two mines. Based on these findings, one can state that the rock samples from Sukari and, in part, from Um Hagalig have a crustal association as they tend to the active continental margin ACM. The obtained findings are in good agreement with the ones found in the literature by Saleh et al. [49]. Similarly, the discrimination diagram of Th-Zr/10-Sc is shown in Figure 9B. The distribution of the mass fractions of the elements on the ternary diagram suggests a slight difference in the geochemistry of the collected samples from Sukari and Um Hagalig, whereas the mass fractions of the elements determined for Hamash locate in the vicinity of granitic gneiss sources.

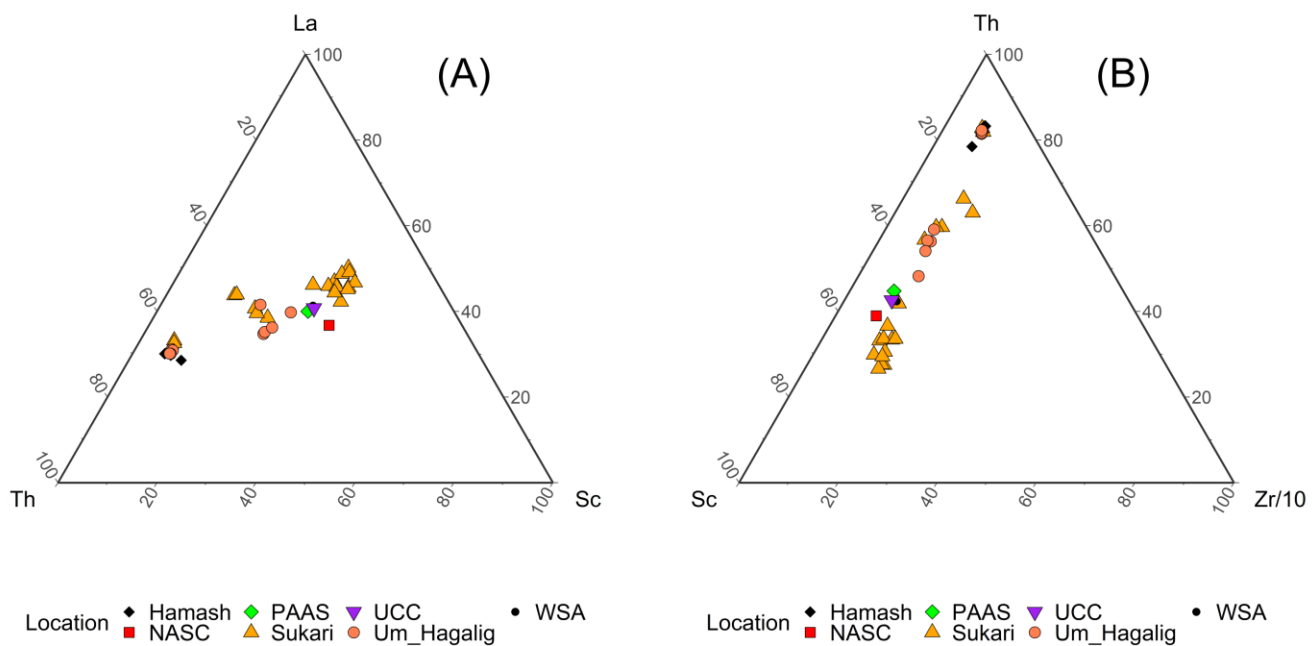


**Figure 9.** (A) a ternary diagram shows the distribution of La-Th-Sc and (B) the distribution of Th-Zr/10-Sc. For comparison purposes, the corresponding values of the elements were considered for UCC by Rudnick and Gao [41], NASC by Gromet, Haskin, Korotev and Dymek [38], Taylor and McLennan [40] for Post Archean Australia Shale PAAS, and Kabata-Pendias [39] for world soil average WSA. Background after Bhatia and Crook [42].

## 6. Conclusions

The objective of the present study was to examine the rock samples collected from gold mines for their elemental composition and metal enrichment. A total of 34, 26, and 33 elements were determined for Sukari, Hamash, and Um Hagalig, respectively. The results obtained show that the mass fractions of the determined elements are significantly higher in the Hamash mine than in Sukari and Um Hagalig. The results were compared with the corresponding values regionally and world-widely. Almost all elements are higher than the corresponding values in UCC, except Au in Sukari mine, which has a lower value compared to Au in Hamash and Um Hagalig. The elements Ca, K, Na, Fe, Zr, Th, and U are dominant and have a significant contribution to the elemental composition of the samples. The comparison of the mean values, based on the analysis of the mass fractions of the determined elements, shows no differences. Multiple ratio indicators analysis revealed that there is high metavolcanics and younger granite recycling for the samples collected at Hamash than the others (Th/Sc versus Zr/Sc). Significant U and Th mass fractions were found in the Hamash mine (Th/U versus Th). The results obtained are comparable to the geochemistry of arc-related felsic volcanic rocks for Hamash and the active continental margin for Sukari and, partially, Um Hagalig. Moreover, the discrimination diagram confirms the findings obtained by the ratio indicators, and there is mostly a remarkable association of the felsic volcanic rocks, most likely accumulated by the Ethiopian highlights.

Therefore, it can be stated that the studied areas are characterized by high mass fractions of U, Th, and rare earth elements, which can be in the interest of Egypt.

**Supplementary Materials:** The following supporting information can be downloaded at: <https://www.mdpi.com/article/10.3390/app13074564/s1>, Table S1: the elemental compositions of the obtained elements in rock samples from the studied areas.

**Author Contributions:** Conceptualization, W.M.B., M.M. and M.S.; methodology, W.M.B. and A.Y.D.; software, W.M.B., O.C. and M.M.; validation, W.M.B., M.M. and M.S.; formal analysis, W.M.B., O.C. and M.M.; investigation, G.S., M.M. and A.E.-F.; resources, W.M.B., M.S. and A.Y.D.; data curation, W.M.B., T.M., M.M. and M.B.; writing—original draft preparation, W.M.B.; writing—review and editing, W.M.B., M.M. and M.S.; visualization, W.M.B.; supervision, W.M.B., A.Y.D. and M.S. All authors have read and agreed to the published version of the manuscript.

**Funding:** This research received no external funding.

**Institutional Review Board Statement:** Not applicable.

**Informed Consent Statement:** Not applicable.

**Data Availability Statement:** The data are provided in this study.

**Acknowledgments:** The authors acknowledge the Academy of Scientific Research and Technology (Egypt) and the Joint Institute for Nuclear Research (Dubna–Russia) ASRT-JINR for the scientific collaboration under the joint research project #382, P.7.

**Conflicts of Interest:** The authors declare no conflict of interest.

## References

- Bierlein, F.P.; Crowe, D. Phanerozoic orogenic lode gold deposits. *Rev. Econ. Geol.* **2000**, *13*, 103–139.
- Goldfarb, R.; Baker, T.; Dubé, B.; Groves, D.I.; Hart, C.J.; Gosselin, P. *Distribution, Character and Genesis of Gold Deposits in Metamorphic Terranes*; Society of Economic Geologists: Ken Caryl, CO, USA, 2005.
- Hassaan, M.; Ramadan, T.; Abu El Leil, I.; Sakr, S. Lithochemical surveys for ore metals in arid region, Central Eastern Desert, Egypt: Using Landsat ETM+ imagery. *Aust. J. Basic Appl. Sci.* **2009**, *3*, 512–528.
- Abd El-Wahed, M.A. Oppositely dipping thrusts and transpressional imbricate zone in the Central Eastern Desert of Egypt. *J. Afr. Earth Sci.* **2014**, *100*, 42–59. [[CrossRef](#)]
- Centamin-plc. *Mineral Resource and Mineral Reserve Estimate for the Sukari Gold Project, Egypt*; Centamin PLC: Saint Helier, Jersey, 2015.
- Centamin-plc. Our Ability to Create Long-Term Value Is Underpinned by The Quality of Our Assets. In *Overview*; Centamin-plc: Saint Helier, Jersey, 2020.
- Egypt-Ministry of Petroleum and Mineral Resources. *The International bid-Round no (1) for the Year 2020 for Exploration of the Gold and Associated Minerals*; Ministry of Petroleum and Mineral Resources: Cairo, Egypt, 2020; *Second Round*.
- Helmy, H.M.; Kaendl, R.; Fritz, H.; Loizenbauer, J. The Sukari Gold Mine, Eastern Desert—Egypt: Structural setting, mineralogy and fluid inclusion study. *MinDe* **2004**, *39*, 495–511. [[CrossRef](#)]
- Abdelaal, A.; Sultan, M.; Elhebiry, M.; Krishnamurthy, R.V.; Sturchio, N. Integrated studies to identify site-specific parameters for environmentally benign mining operations: A case study from the Sukari Gold Mine, Egypt. *Sci. Total Environ.* **2021**, *750*, 141654. [[CrossRef](#)]
- El-Desoky, H.M.; Shahin, T.M.; Amer, Y.Z. Characteristic of gold mineralization associated with granites at Hamash old gold mine, South Eastern Desert, Egypt. *Arab. J. Geosci.* **2021**, *14*, 558. [[CrossRef](#)]
- Botros, N. The role of the granite emplacement and structural setting on the genesis of gold mineralization in Egypt. *Ore Geol. Rev.* **2015**, *70*, 173–187. [[CrossRef](#)]
- Zoheir, B. Transpressional zones in ophiolitic mélange terranes: Potential exploration targets for gold in the South Eastern Desert, Egypt. *J. Geochem. Explor.* **2011**, *111*, 23–38. [[CrossRef](#)]
- Saleh, G.M.; Mitwalli, M.E.-S.; Yousef, H.A.; El farrash, A.H. Environmental Radioactivity of Radon and its Hazards in Hamash Gold Mine, Egypt. *Arab J. Nucl. Sci. Appl.* **2019**, *52*, 190–196. [[CrossRef](#)]
- Abd El-Wahed, M.A.; Harraz, H.; El-Behairy, M.H. Transpressional imbricate thrust zones controlling gold mineralization in the Central Eastern Desert of Egypt. *Ore Geol. Rev.* **2016**, *78*, 424–446. [[CrossRef](#)]
- Lundmark, A.M.; Andresen, A.; Hassan, M.A.; Augland, L.E.; Boghdady, G.Y. Repeated magmatic pulses in the East African Orogen in the Eastern Desert, Egypt: An old idea supported by new evidence. *Gondwana Res.* **2012**, *22*, 227–237. [[CrossRef](#)]
- Mitwalli, M.; Badway, W.; Yosef, H.; Salama, S.; Saleh, G.; El-Farrash, A.H. Radon Measurement and Radiological Dose Assessment From Terrestrial Rocks Using Solid-State Nuclear Track Detectors. *Arab J. Nucl. Sci. Appl.* **2022**, 1–8. [[CrossRef](#)]
- Bode, P. Neutron Activation Analysis (NAA). In *Neutron Methods for Archaeology and Cultural Heritage*; Kardjilov, N., Festa, G., Eds.; Springer International Publishing: Cham, Switzerland, 2017; pp. 209–219.

18. Frontasyeva, M.V. Neutron activation analysis in the life sciences. *Phys. Part. Nucl.* **2011**, *42*, 332–378. [[CrossRef](#)]
19. Arafa, W.M.; Badawy, W.M.; Fahmi, N.M.; Ali, K.; Gad, M.S.; Duliu, O.G.; Frontasyeva, M.V.; Steinnes, E. Geochemistry of sediments and surface soils from the Nile Delta and lower Nile valley studied by epithermal neutron activation analysis. *J. Afr. Earth Sci.* **2015**, *107*, 57–64. [[CrossRef](#)]
20. Badawy, W.M.; El-Taher, A.; Frontasyeva, M.V.; Madkour, H.A.; Khater, A.E.M. Assessment of anthropogenic and geogenic impacts on marine sediments along the coastal areas of Egyptian Red Sea. *Appl Radiat Isot* **2018**, *140*, 314–326. [[CrossRef](#)]
21. Badawy, W.M.; Duliu, O.G.; Frontasyeva, M.V.; El-Samman, H.; Mamikhin, S.V. Dataset of elemental compositions and pollution indices of soil and sediments: Nile River and delta -Egypt. *Data Brief* **2020**, *28*, 105009. [[CrossRef](#)]
22. Badawy, W.M.; Duliu, O.G.; El Samman, H.; El-Taher, A.; Frontasyeva, M.V. A review of major and trace elements in Nile River and Western Red Sea sediments: An approach of geochemistry, pollution, and associated hazards. *Appl Radiat Isot* **2021**, *170*, 109595. [[CrossRef](#)]
23. Badawy, W.M.; Sarhan, Y.; Duliu, O.G.; Kim, J.; Yushin, N.; Samman, H.E.; Hussein, A.A.; Frontasyeva, M.; Shcheglov, A. Monitoring of air pollutants using plants and co-located soil-Egypt: Characteristics, pollution, and toxicity impact. *Environ. Sci. Pollut. Res. Int.* **2022**, *29*, 21049–21066. [[CrossRef](#)]
24. IAEA. *Soil Sampling for Environmental Contaminants*; International Atomic Energy Agency: Vienna, Austria, 2004.
25. Gaby, S.E.; List, F.K.; Tehrani, R. The basement complex of the Eastern Desert and Sinai. In *The Geology of Egypt*, 1st ed.; Routledge: London, UK, 1990.
26. Koval, V.Y.; Dmitriev, A.Y.; Borzakov, S.B.; Chepurchenko, O.E.; Filina, Y.G.; Smirnova, V.S.; Lobachev, V.V.; Chepurchenko, N.N.; Bulavin, M.V. Ceramics of Bolgar: The First Results of Usage of Neutron Activation Analysis. *Phys. Part. Nucl. Lett.* **2019**, *16*, 1004–1020. [[CrossRef](#)]
27. Bulavin, M.; Cheplakov, A.; Kukhtin, V.; Kulagin, E.; Kulikov, S.; Shabalin, E.; Verkhoglyadov, A. Irradiation facility at the IBR-2 reactor for investigation of material radiation hardness. *Nucl. Instrum. Methods Phys. Res. Sect. B: Beam Interact. Mater. At.* **2015**, *343*, 26–29. [[CrossRef](#)]
28. Badawy, W.M.; Dmitriev, A.Y.; Koval, V.Y.; Smirnova, V.S.; Chepurchenko, O.E.; Lobachev, V.V.; Belova, M.O.; Galushko, A.M. Formation of reference groups for archaeological pottery using neutron activation and multivariate statistical analyses. *Archaeol. Sci.* **2022**, *64*, 1377–1393. [[CrossRef](#)]
29. Barandovski, L.; Frontasyeva, M.V.; Stafilov, T.; Šajin, R.; Ostrovnyaya, T.M. Multi-element atmospheric deposition in Macedonia studied by the moss biomonitoring technique. *Environ. Sci. Pollut. Res.* **2015**, *22*, 16077–16097. [[CrossRef](#)] [[PubMed](#)]
30. Dmitriev, A.Y.; Pavlov, S.S. Automation of the quantitative determination of elemental content in samples using neutron activation analysis on the IBR-2 reactor at the Frank Laboratory for Neutron Physics, Joint Institute for Nuclear Research. *Phys. Part. Nucl. Lett.* **2013**, *10*, 33–36. [[CrossRef](#)]
31. R Core Team. *R: A Language and Environment for Statistical Computing*; R Foundation for Statistical Computing; R Core Team: Vienna, Austria, 2020.
32. Shapiro, S.S.; Wilk, M.B. An analysis of variance test for normality (complete samples). *Biometrika* **1965**, *52*, 591–611. [[CrossRef](#)]
33. Haynes, W. Tukey's Test. In *Encyclopedia of Systems Biology*; Dubitzky, W., Wolkenhauer, O., Cho, K.-H., Yokota, H., Eds.; Springer: New York, NY, USA, 2013; pp. 2303–2304.
34. Tukey, J.W. *Exploratory Data Analysis*; Addison-Wesley: Boston, CA, USA, 1977.
35. Reimann, C.; Filzmoser, P. Normal and lognormal data distribution in geochemistry: Death of a myth. Consequences for the statistical treatment of geochemical and environmental data. *Environ. Geol.* **2000**, *39*, 1001–1014. [[CrossRef](#)]
36. Anderson, D.R. *Model Based Inference in the Life Sciences: A Primer on Evidence*, 1st ed.; Springer: New York, NY, USA, 2008.
37. Roshdy, O.E.; Haggag, E.A.; Masoud, A.M.; Bertau, M.; Haneklaus, N.; Pavón, S.; Hussein, A.E.M.; Khawassek, Y.M.; Taha, M.H. Leaching of rare earths from Abu Tartur (Egypt) phosphate rock with phosphoric acid. *J. Mater. Cycles Waste Manag.* **2023**, *25*, 501–517. [[CrossRef](#)]
38. Gromet, L.P.; Haskin, L.A.; Korotev, R.L.; Dymek, R.F. The “North American shale composite”: Its compilation, major and trace element characteristics. *Geochim. Et Cosmochim. Acta* **1984**, *48*, 2469–2482. [[CrossRef](#)]
39. Kabata-Pendias, A. *Trace Elements in Soils and Plants*, 4th ed.; CRC Press: Boca Raton, FL, USA, 2011; p. 548.
40. Taylor, S.R.; McLennan, S.M. *The Continental Crust, Its Composition and Evolution: An Examination of the Geochemical Record Preserved in Sedimentary Rocks*; Blackwell Scientific: Oxford, UK, 1985; p. 312.
41. Rudnick, R.L.; Gao, S. Composition of the Continental Crust. In *Treatise on Geochemistry*; Turekian, K.K., Ed.; Elsevier: Oxford, UK, 2014; pp. 1–51.
42. Bhatia, M.R.; Crook, K.A.W. Trace element characteristics of graywackes and tectonic setting discrimination of sedimentary basins. *Contrib. Mineral. Petrol.* **1986**, *92*, 181–193. [[CrossRef](#)]
43. Mironov, A.G.; Zhmodic, S.M.; Ochirov, Y.C. Determination of gold and uranium mineralization in black schists and sulfide ores using radiography complex. *Radiat. Measur.* **1995**, *25*, 495–498. [[CrossRef](#)]
44. Zhu, Y.; An, F.; Tan, J. Geochemistry of hydrothermal gold deposits: A review. *Geosci. Front.* **2011**, *2*, 367–374. [[CrossRef](#)]
45. Verma, S.P.; Armstrong-Altrin, J.S. New multi-dimensional diagrams for tectonic discrimination of siliciclastic sediments and their application to Precambrian basins. *Chem. Geol.* **2013**, *355*, 117–133. [[CrossRef](#)]
46. Armstrong-Altrin, J.S.; Verma, S.P. Critical evaluation of six tectonic setting discrimination diagrams using geochemical data of Neogene sediments from known tectonic settings. *Sediment. Geol.* **2005**, *177*, 115–129. [[CrossRef](#)]

47. Pearce, J.A.; Harris, N.B.W.; Tindle, A.G. Trace Element Discrimination Diagrams for the Tectonic Interpretation of Granitic Rocks. *JPet* **1984**, *25*, 956–983. [[CrossRef](#)]
48. Schandl, E.S.; Gorton, M.P. Application of High Field Strength Elements. *Econ. Geol.* **2002**, *97*, 629–642. [[CrossRef](#)]
49. Saleh, G.M.; Khaleal, F.M.; Lasheen, E.S.R. Geochemistry and paleoweathering of metasediments and pyrite-bearing quartzite during the Neoproterozoic Era, Wadi Ibib-Wadi Suwawrib, South Eastern Desert, Egypt. *Arab. J. Geosci.* **2021**, *15*, 51. [[CrossRef](#)]

**Disclaimer/Publisher’s Note:** The statements, opinions and data contained in all publications are solely those of the individual author(s) and contributor(s) and not of MDPI and/or the editor(s). MDPI and/or the editor(s) disclaim responsibility for any injury to people or property resulting from any ideas, methods, instructions or products referred to in the content.